

Development of Plasma Parameters for the Manufacture of MCrAlY Bond Coats by Low-Pressure Plasma Spraying Using a Cascaded Torch

Georg Mauer

MCrAlY bond coats (M=Ni, Co) for thermal barrier coating systems are often manufactured by low-pressure plasma spraying (LPPS) to achieve dense coatings with low oxygen uptake at high deposition efficiencies. Herein, the novel SinplexPro 03C plasma spray torch (Oerlikon Metco) is characterized regarding this application, and appropriate process parameters are developed. The mass-specific plasma enthalpy and the hydrogen–argon plasma gas ratio prove to be substantial factors. The best deposition efficiency and lowest porosity are achieved at a mass-specific plasma enthalpy between 17 and 19 MJ kg^{−1}. The oxygen content increases degressively with the enthalpy. Already at small hydrogen fractions in the plasma gas, a fast route is established for the recombination of argon ions. Consequently, the thermal treatment of the feed-stock is improved. Moreover, the porosity decreases at increasing hydrogen content of the plasma gas, as the gun is operated in constant current mode and thus the input power increases. However, the deposition efficiency decreases slightly. On the other hand, the oxygen content decreases due to the reducing effect of hydrogen. The deposition efficiency, porosity, and oxygen content are also reasonable if no hydrogen is admixed at all, as the fluctuations of the plasma are reduced.

1. Introduction


MCrAlY-type bond coats (M=Co, Ni) are commonly used to protect metallic substrates from oxidation and to improve adhesion of ceramic thermal barrier coatings (TBCs) for high-temperature applications such as land-based gas turbines and aero engines. During service, an alumina-based oxide scale (thermally grown

oxide, TGO) is formed at the bond coat surface. A dense TGO can prevent oxygen from diffusing into the bond coat so that underlying structural alloys are protected from high-temperature oxidation and corrosion attack.^[1] Besides the MCrAlY composition (major elements Co, Ni, Al, and Cr as well as minor additions of reactive elements such as Y, La, Hf, Zr, Ca, Si, etc.), atmosphere composition,^[2] exposure conditions,^[3] and surface conditions^[4] can have considerable effects on the bond coat performance. Among manufacturing related parameters,^[5] the spray process is of particular importance^[6] as MCrAlY particles are prone to take up oxygen during flight and cooling down after deposition. Consequently, the formation of Al-rich oxides lowers the metallic Al concentration, which is available for diffusion and TGO formation. This is generally assumed to affect the oxidation resistance adversely. In contrast, if the oxygen content is too low, only small amounts of reactive elements (RE) like Y are tied up so that

RE overdoping may occur, increasing the TGO growth and thus affecting TBC lifetimes negatively.^[7]

In Shibata et al.,^[8] oxygen contents of 0.16, 0.94, and 1.8 wt% are reported for CoNiCrAlY coatings manufactured by low-pressure plasma spraying (LPPS, formerly termed vacuum plasma spraying, VPS), high-velocity oxy-fuel spraying (HVOF), and atmospheric plasma spraying (APS), respectively. Similar values (0.9 wt% in CoNiCrAlY) are given in ref. [9] for HVOF spraying and in ref. [10] (0.4–0.7 wt% in NiCoCrAlY). In ref. [11], it is reported that even lower (<0.3 wt%) oxygen content can be achieved by HVOF spraying if coarser powder cuts are used (−75/+45 μm). However, this was associated with significant higher porosities. CoNiCrAlY bond coats with similar oxygen contents (≈0.4 wt%) and high oxidation resistance were obtained by a novel high kinetic spray process termed as high-velocity atmospheric plasma spraying (HV-APS).^[12] Cold gas spraying (CGS) is another innovative kinetic process that is expected to yield very low oxygen levels due to its low process temperatures.^[13] For MCrAlY alloys however, this turned out to be challenging, as the deposition efficiencies were poor^[14] so that some researchers either used helium as process gas,^[15] which is hardly accepted in industry, or applied laser assistance.^[16] Hence, if high deposition efficiencies are required, a

G. Mauer
Institute of Energy and Climate Research
IEK-1: Materials Synthesis and Processing
Forschungszentrum Jülich GmbH
52428 Jülich, Germany
E-mail: g.mauer@fz-juelich.de

 The ORCID identification number(s) for the author(s) of this article can be found under <https://doi.org/10.1002/adem.202200856>.

© 2022 The Authors. Advanced Engineering Materials published by Wiley-VCH GmbH. This is an open access article under the terms of the Creative Commons Attribution-NonCommercial-NoDerivs License, which permits use and distribution in any medium, provided the original work is properly cited, the use is non-commercial and no modifications or adaptations are made.

DOI: 10.1002/adem.202200856

promising option is still working under inert gas conditions at low pressure by LPPS reaching oxygen contents in MCrAlY coatings less than 0.1 wt%.^[17]

Regarding the LPPS process, the F4-VB torch and the 03CP torch (Oerlikon Metco) were the workhorses for some decades. The latter is usually used for large components as they can be kept at a higher coating temperature to achieve good adhesion due to the higher torch power. These noncascaded single-cathode guns are robust and relatively simple but typically also sensitive to aging. If operated in a constant current mode, the torch voltage continuously drops requiring the replacement of the electrodes in time.^[18] Another characteristic of such single-cathode torches is the pronounced fluctuation of the arc. Depending on the torch power and the amount of molecular secondary plasma gas (H_2 , N_2), these torches operate in the so-called restrike mode.^[19] Here, the arc dynamics are a prime source of broadening the distribution of the particle in-flight characteristics. This can lead to a higher content of partially or not melted particles and thus to an increased porosity and lower deposition efficiency.^[20]

Consequently, multielectrode plasma torches were designed to improve the operation stability and lifetime with respect to single-cathode guns.^[21] In this context, also cascaded nozzles were introduced limiting effectively the movements of the anodic arc attachment in axial direction.^[22] Such kind of design comprises a stack of neutrodes in front of the anode, which are electrically insulated from each other. This makes it possible to achieve an arc length longer than the average so-called self-setting length (controlled by the arc current, composition, and flow rate of the plasma gas and electrode geometry).^[23] As the arc behaves more stable, the power demand is virtually constant and the treatment of the feedstock particle is uniform in contrast

to legacy noncascaded torches. **Figure 1** shows schematic illustrations of these two torch concepts.

The SinplexPro (Oerlikon Metco) is an approach to incorporate the advantages of the cascaded arc technology also into a single-cathode spray gun.^[24] The SinplexPro 03C is the low pressure-compatible variant that can be operated at chamber pressures down to 3 kPa; the maximum allowed power is 130 kW at a maximum current of 1200 A. The hydrogen–argon ratio in the plasma gas should not exceed 0.1 up to an argon flow of 80 slpm and 0.125 above until 130 slpm Ar; preferentially, it should be lower (≤ 0.05 – 0.06). In this work, plasma parameters were developed for the manufacture of MCrAlY bond coats by LPPS with this torch. Some experiments with the F4-VB gun were carried out for comparison. Color-edited photographs and optical emission spectroscopy (OES) were used to characterize the plasma jets in order to find explanations for the observed results.

2. Results and Discussion

Two sets of experiments were performed to follow different directions in the development of plasma parameters for the SP-03C torch. Furthermore, some tests with the F4-VB gun were made for comparison.

2.1. The Effect of Plasma Enthalpy

The first investigated parameter SP-1.1 for the SP-03C torch was selected according to the tested and proven parameter F4-1 for bond coats with the F4-VB torch (see **Table 1**). The electrical

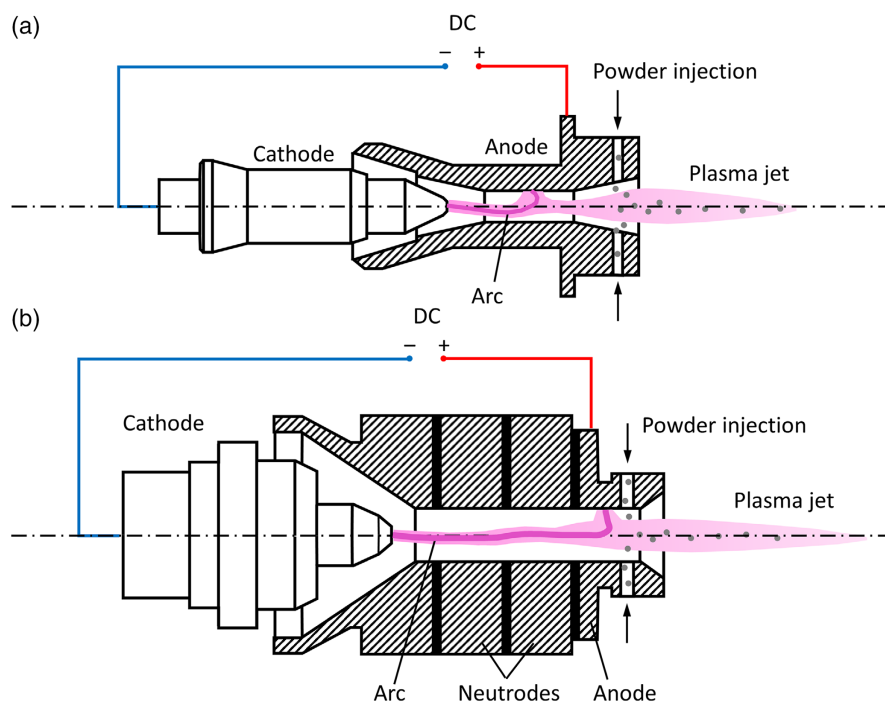


Figure 1. a) Schematic illustrations (not to scale) of a noncascaded legacy plasma spray torch like the F4-VB, and b) a cascaded torch like the SP-03C used in this work.

Table 1. Investigated process parameters for spray experiments.

| Set | Current [A] | Ar [slpm] ^{a)} | H ₂ [slpm] ^{a)} | P _{in} [kW] | P _{net} [kW] | h [MJ kg ⁻¹] | S/D [mm] | P _{chamber} [kPa] |
|--------|----------------|----------------------------|--|-------------------------|--------------------------|-----------------------------|-------------|-------------------------------|
| F4-1 | 640 | 50 | 9 | 43.8 | 25.7 | 17.1 | 275 | 6 |
| SP-1.1 | 620 | 50 | 5 | 46.9 | 28.1 | 18.8 | 470 | 6 |
| SP-1.2 | 500 | 110 | 11 | 47.0 | 30.6 | 9.3 | 275 | 6 |
| SP-1.3 | 800 | 50 | 2.5 | 59.6 | 35.5 | 23.8 | 500 | 6 |
| SP-2.1 | 810 | 100 | 5 | 75.5 | 49.6 | 16.6 | 500 | 4 |
| SP-2.2 | 880 | 100 | 0 | 75.3 | 51.1 | 17.2 | 500 | 4 |
| SP-2.3 | 780 | 100 | 10 | 77.5 | 49.1 | 16.4 | 500 | 4 |

^{a)}Standard liters per minute.

input power and mass-specific plasma enthalpy were chosen similarly. For these parameters, the torch efficiency, i.e., the ratio of the plasma net power and the electrical input power, turned out to be just a little higher for the SP-03C (60%) than for the F4-VB (58%). However, the spray distance had to be increased from 275 mm for the F4-VB to 470 mm, as the jet was distinctly longer. **Figure 2** shows the image processing of the F4-VB plasma jet using the parameter F4-1. **Figure 3** shows an image sequence of the plasma jet color-edited in the same way using the SP-03C torch with parameter SP-1.1. Looking at the development of the jet diameters near the nozzle exits and at the overall jet structures, it is obvious that both jets are underexpanded. At the chamber pressure of 6 kPa however, the F4-VB torch operated closer to the design pressure than the SP-03C.

In addition to the mentioned starting parameter, SP-1.1, the effect of higher plasma gas flow was investigated with parameter SP-1.2. While the total plasma gas flow was more than doubled, the torch input power was kept on constant level by reducing the current. With this, the torch efficiency increased to 65%. The same short spray distance of 275 mm could be used as with the F4-VB torch. A further experiment with parameter SP-1.3 focused on the effect of raising the current while the hydrogen fraction in the plasma gas was halved. Here, the jet was much longer so that the spray distance had to be enlarged to 500 mm. The torch efficiency was the same as with SP-1.1. **Figure 4** and **5** show image sequences with edited colors of the plasma jets with parameter SP-1.2 and SP-1.3. In the first case

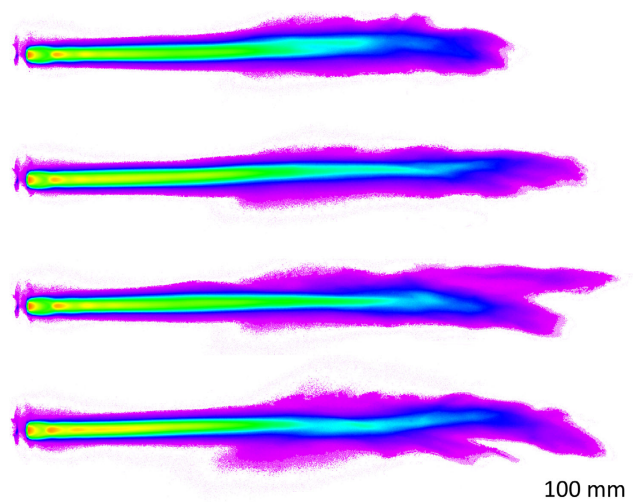


Figure 3. Sequence with pseudocolor images of the plasma jet using the SP-03C torch with parameter SP-1.1.

with the high plasma gas flow, the net plasma power increased slightly but due to the considerably reduced mass-specific plasma enthalpy, the jet length decreased distinctly. In the other case, SP-1.3, the jet length increased and more shock diamonds could be observed. Pronounced fluctuations were evident although the hydrogen gas flow was halved with respect to SP-1.1.

The results of this first set of spray experiments with the powder Amdry 386 and the parameters F4-1, SP-1.1, SP-1.2, and SP-1.3 are given in **Figure 6**. It turned out that the best results for the SP-03C torch were obtained with parameter SP-1.1. However, for this setting, the deposition efficiencies were not that high and the oxygen content was not that low as achieved with the F4-VB torch while the porosity was the lowest. Comparing the SP-03C results, the high porosity and somewhat lower deposition efficiency found for parameter SP-1.2, where the gas flow was increased at the same power as parameter SP-1.1, are associated with the low mass-specific plasma enthalpy. The short jet length was an indication for this. For parameter SP-1.3, where the power was changed by raising the current and halving the hydrogen flow with respect to parameter SP-1.1, the strong fluctuations due to the high mass-specific plasma enthalpy are assumed as

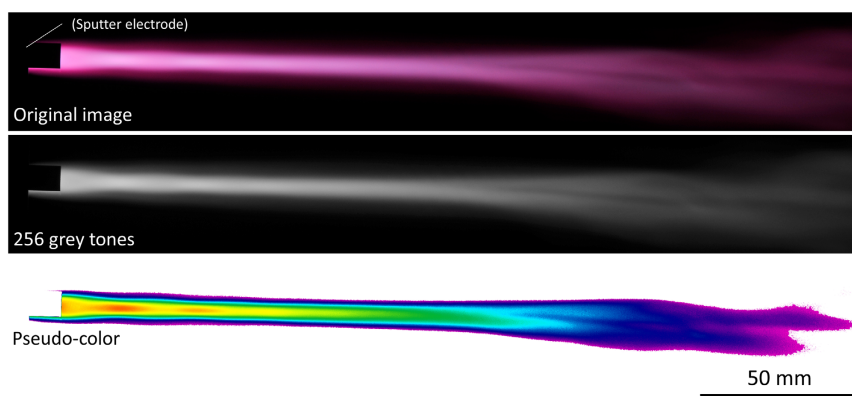


Figure 2. Image processing of the F4-VB plasma jet using the example of parameter F4-1.

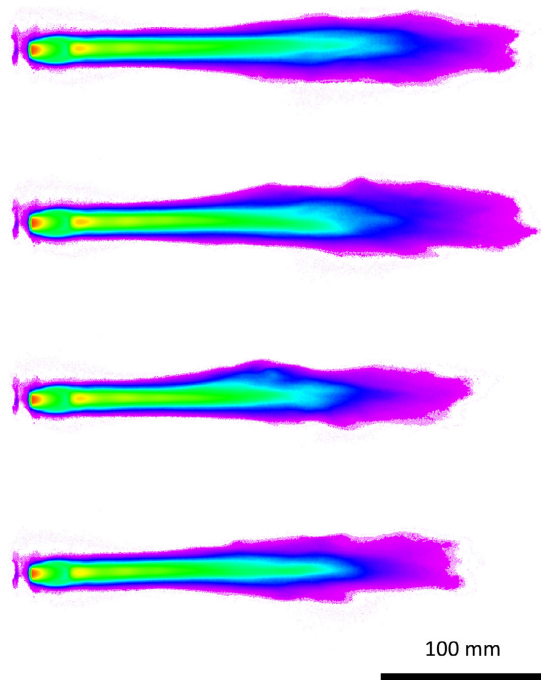


Figure 4. Sequence with pseudocolor images of the plasma jet using the SP-03C torch with parameter SP-1.2.

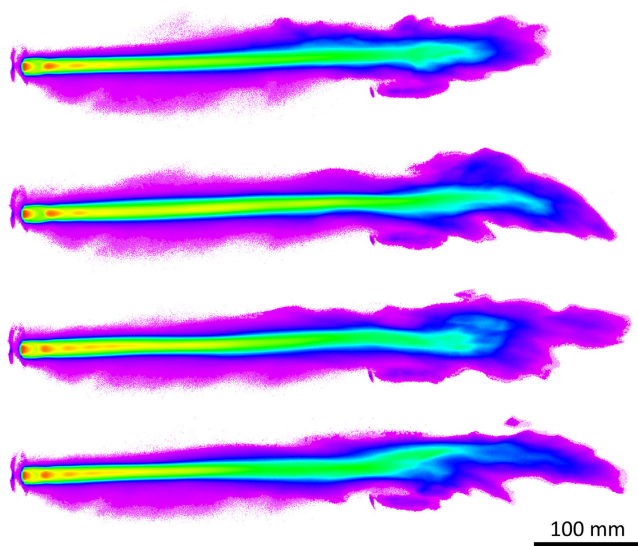


Figure 5. Sequence with pseudocolor images of the plasma jet using the SP-03C torch with parameter SP-1.3.

reason why porosities and deposition efficiencies could not be improved with respect to parameter SP-1.1. These two characteristic values show a more or less well-developed optimum at a mass-specific plasma enthalpy between 17 and 19 MJ kg⁻¹. The oxygen content increased with the SP-03C torch degressively as the mass-specific enthalpy was raised. The lowest value for parameter SP-1.2 corresponds to the reference value obtained with the F4-VB gun.

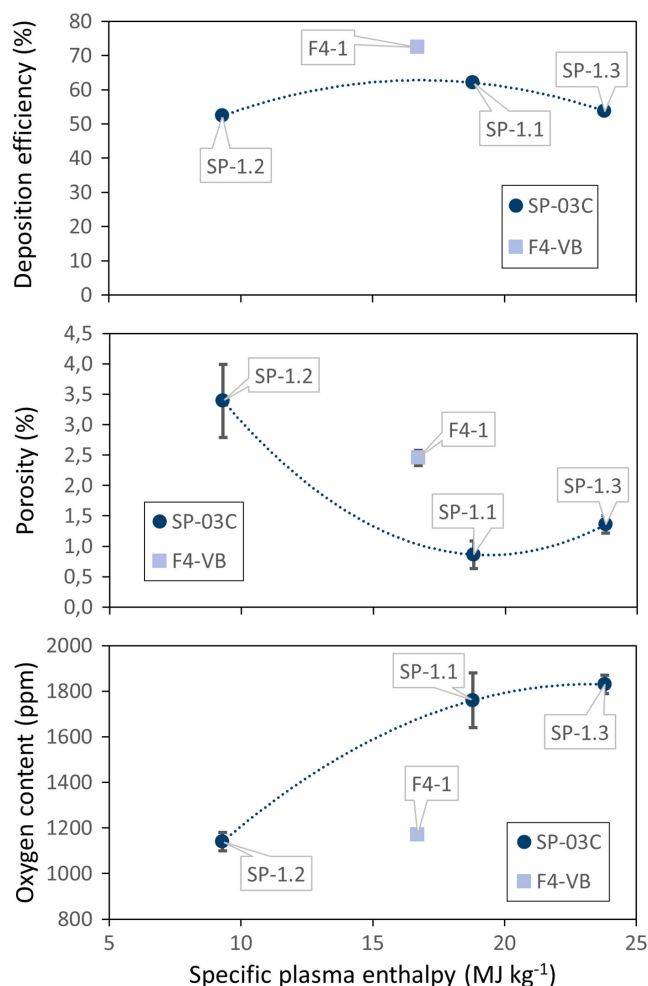


Figure 6. Results of spray experiments with the feedstock powder Amdry 386.

Figure 7 shows cross sections of the sprayed samples with parameters SP-1.1, SP-1.2, SP-1.3, and F4-1. The microstructures do not show any partly or nonmolten particles. In fact, full particle melting could be expected for MCrAlY under the investigated spray conditions. The different porosity levels are evident and the ranking in deposition efficiency is comprehensible looking at the porosities and coating thicknesses. There are no visible oxides.

2.2. The Effect of Hydrogen–Argon Ratio

The effect of the hydrogen–argon ratio in the plasma gas was investigated in the next set of experiments with the powder Amdry 9954 and parameters F4-1, SP-2.2, SP-2.2, and SP-2.3 (see Table 1). For all cases, the mass-specific plasma enthalpy was maintained on a virtually constant level at approximately 17 MJ kg⁻¹. For the SP-03C torch, this was achieved by adjusting the current while the hydrogen flow was varied between 0 and 10 slpm and the argon flow was constant. Compared to the starting parameter SP-1.1, argon was increased to 100 slpm with the

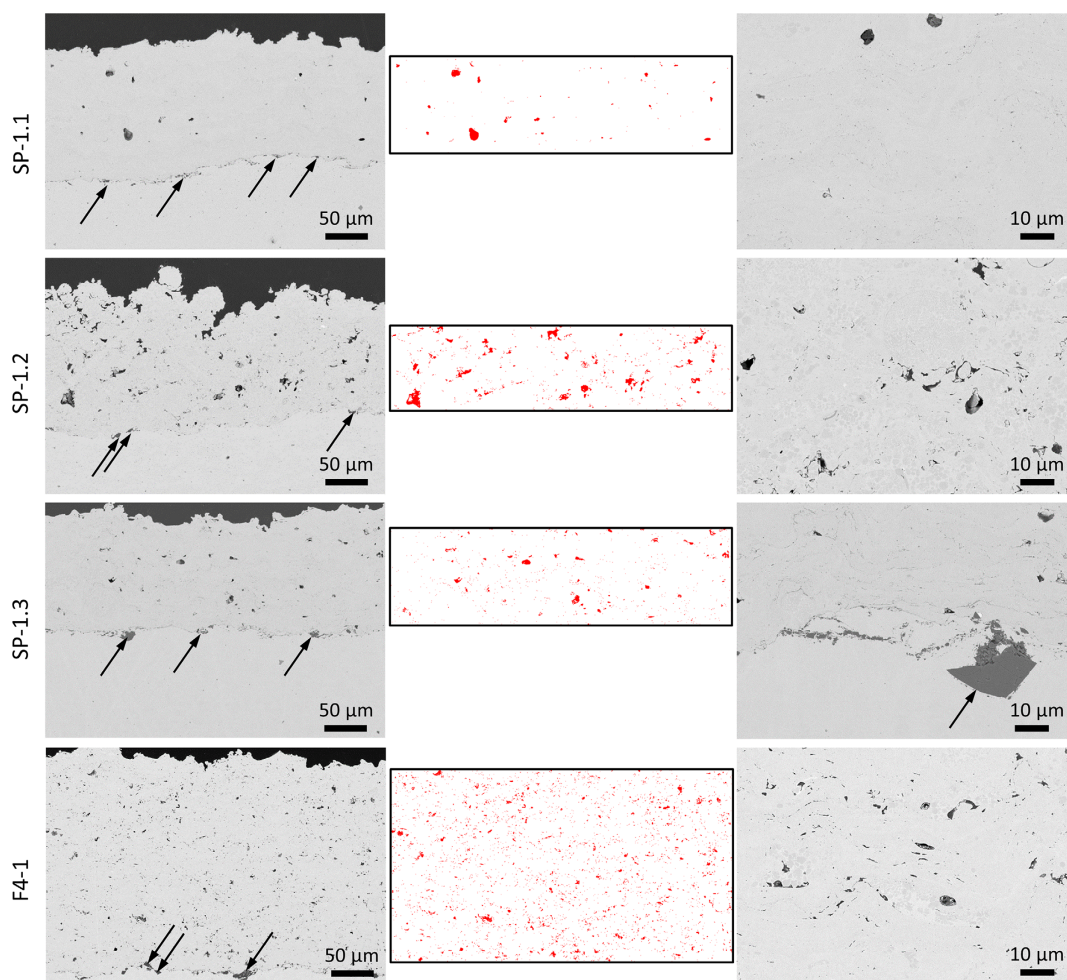


Figure 7. Microstructures of the sprayed samples with the powder Amdry 386 and parameters SP-1.1, SP-1.2, SP-1.3, and F4-1 (backscattered electron images); arrows indicate alumina grits left behind from blasting; threshold graphs for porosity determination of the images in the left column are given in the middle.

intention to obtain denser coatings with better deposition efficiencies. Thus, the currents generally had to be chosen higher as for parameter SP-1.1 as well. The chamber pressure was reduced to 4 kPa to lower the oxygen partial pressure.

Compared to the first set of experiments, the overall torch efficiency of the SP-03C gun improved to 63–68% in this second set. The results are given in **Figure 8**. The porosities were found to be slightly increased which may be related to the somewhat larger particles of the Amdry 9954 feedstock. Unexpectedly, the deposition efficiencies were generally lower. Compared to parameter SP-2.1, in the case of the pure argon parameter SP-2.2, the low plasma fluctuation is assumed to improve the deposition efficiency and to a small extent the porosity. In the case of the highest content of hydrogen at parameter SP-2.3, the increased thermal conductivity and thus better particle treatment are suggested to be the reason for the lower porosities than for parameter SP-2.1. Thus, the mass-specific plasma enthalpy (see Section 2.1), which was kept virtually constant in this set of experiments, is not the only significant parameter, but secondarily, also the hydrogen content has an impact, namely, on the

porosity. The porosity obtained for the reference sample F4-1 sprayed was on a similar level as for the SP-03C samples, while the high deposition efficiency and the low oxygen content of the F4-1 sample were not reached. This turned out also in the first experiment set.

Compared to the first set of spray series, the oxygen contents in the coatings were consistently slightly lower because the Amdry 9954 feedstock is less prone for oxygen uptake than Amdry 386 due to the different chemical compositions. Another reason may be the slightly lower chamber pressure. The lowest oxygen content in this set of experiments at virtually constant plasma enthalpy is achieved for the highest hydrogen fraction, parameter SP-2.3. It corresponds to the value of the reference sample sprayed with the F4-VB torch. A reducing effect is assumed as reason for this. On the other hand, the pure argon parameter SP-2.2 without any hydrogen also had a little lower oxygen content as result than parameter SP-2.1 which might be due to the smaller jet fluctuation and length. Thus, besides the plasma enthalpy (see Section 2.1), the hydrogen content affects the oxygen content as well.

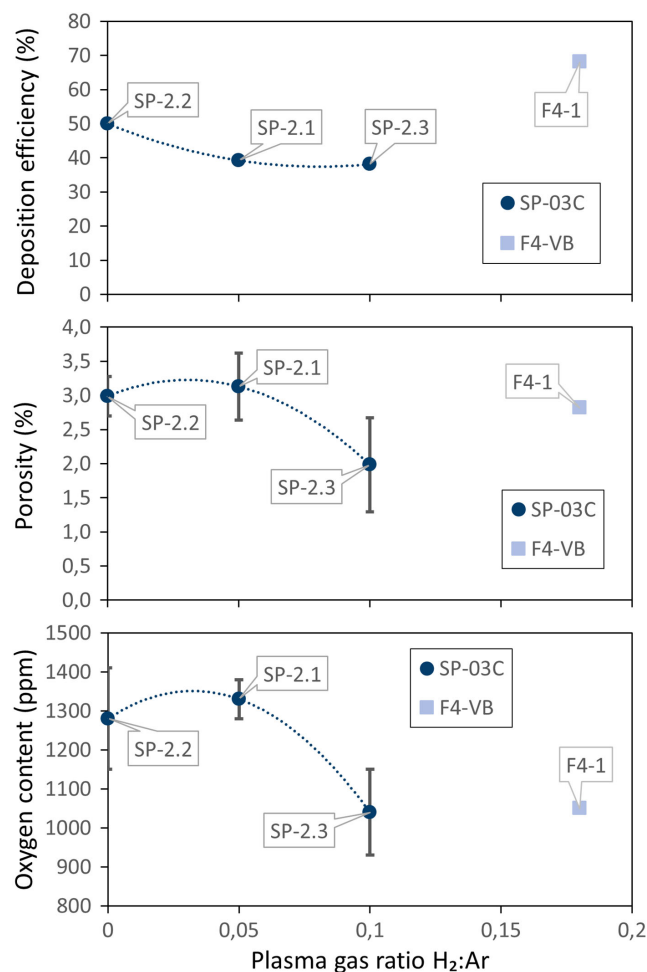


Figure 8. Results of spray experiments with the feedstock powder Amdry 9954.

Figure 9 shows cross sections of the sprayed samples with parameters SP-2.1, SP-2.2, SP-2.3, and F4-1. Again, the different porosity levels are evident and the ranking in deposition efficiency is comprehensible looking at the porosities and coating thicknesses. There are also no visible oxides as before.

OES was performed to shed some light on the role of hydrogen in the plasma gas. To improve the measurement conditions, the lower chamber pressure of 4 kPa was selected in all cases. The current was reduced to 500 A for the SP-03C torch and set to 650 A for the F4-VB-torch. This gave virtually the same torch input powers if both guns were operated with 5 slpm hydrogen. The plasma gas compositions were the same as for parameters SP-2.1, SP-2.2, and SP-2.3, but as hydrogen spectral lines were evaluated, the hydrogen flow could not be reduced to 0 slpm; instead, 1 slpm was set. Comparing the results for the SP-03C torch with different hydrogen flows at constant argon flow and current, it must be noted that the hydrogen addition results in an increase of the torch input power; for 1, 5, and 10 slpm hydrogen, 36.7, 41.7, and 45.8 kW were obtained, respectively. In the F4 reference case, it was 41.3 kW, which is in the mid of that range.

Figure 10 gives radial profiles of the excitation temperature at 340 mm downstream from the nozzle for the plasma parameters SP-3.1, SP-3.2, and SP-3.3, and for the reference case F4-2. They can be equated with the electron temperatures and with the heavy species' temperatures of atoms and ions if local thermal equilibrium (LTE) presumes. The electron densities are shown in **Figure 11**, and **Figure 12** gives the concentration ratios of hydrogen and neutral argon species.

With increasing hydrogen content, the plasma conditions become strongly recombining.^[25] On the basis of experimental^[26] and modeling^[27] results, it was suggested that soon after onset of jet expansion an associative charge exchange of Ar⁺ and H₂ occurs



This is followed by the dissociative recombination of the produced ArH⁺



Consequently, a strong decrease of Ar* line intensities and dominant H* lines are observed in the spectra (* indicates the excited states). Besides Ar*, also the Ar⁺ line intensities decrease significantly when hydrogen is added to the plasma gas. This confirms the proposed recombination route, which is very effective.^[28]

The excitation temperatures were increased due to the presence of hydrogen as this fast recombination route emerged; in contrast, the reactive part of the thermal conductivity was enhanced by hydrogen, resulting in a more effective radial heat dissipation. Thus, comparing hydrogen additions of 1, 5, and 10 slpm with the SP-03C torch (parameters SP-3.1, SP-3.2, and SP-3.3), the highest temperatures were observed at the medium H₂ admixture of 5 slpm (SP-3.2) (**Figure 10**). The temperature distribution for the F4-VB torch is more concentrated toward the jet axis than for the SP-03C gun. This could be an indication that the recombination is less effective; furthermore, the different nozzle diameters may be another reason for this.

As hydrogen is added, the ionization degree and thus the electron density are reduced via recombination.^[29] On the other hand, the torch input power and consequently the ionization degree increased because the current was kept constant as mentioned above. Obviously, both effects on the electron density cancel each other (**Figure 11**). For the F4-VB torch (parameter F4-2), slightly higher values are obtained which might be an indication again that the recombination does not progress as effectively as with the SP-03C torch (parameters SP-3.1, SP-3.2, and SP-3.3).

The local composition of the expanding plasma jet varied considerably (**Figure 12**). It is trivial that the hydrogen concentrations generally increased if more hydrogen was added (SP-3.1 to SP-3.3). Comparing the SP-03C and the F4-VB torch both with 10% hydrogen addition (SP-3.3 and F4-2), the hydrogen concentration is lower in the latter case. As only excited hydrogen species H* contribute to the evaluated emission peak, it can be assumed again that the mentioned recombination reactions producing excited hydrogen species H* were less efficient than with the SP-03C torch. The radial distributions of the concentrations show that hydrogen atoms obviously escaped from the jet core in

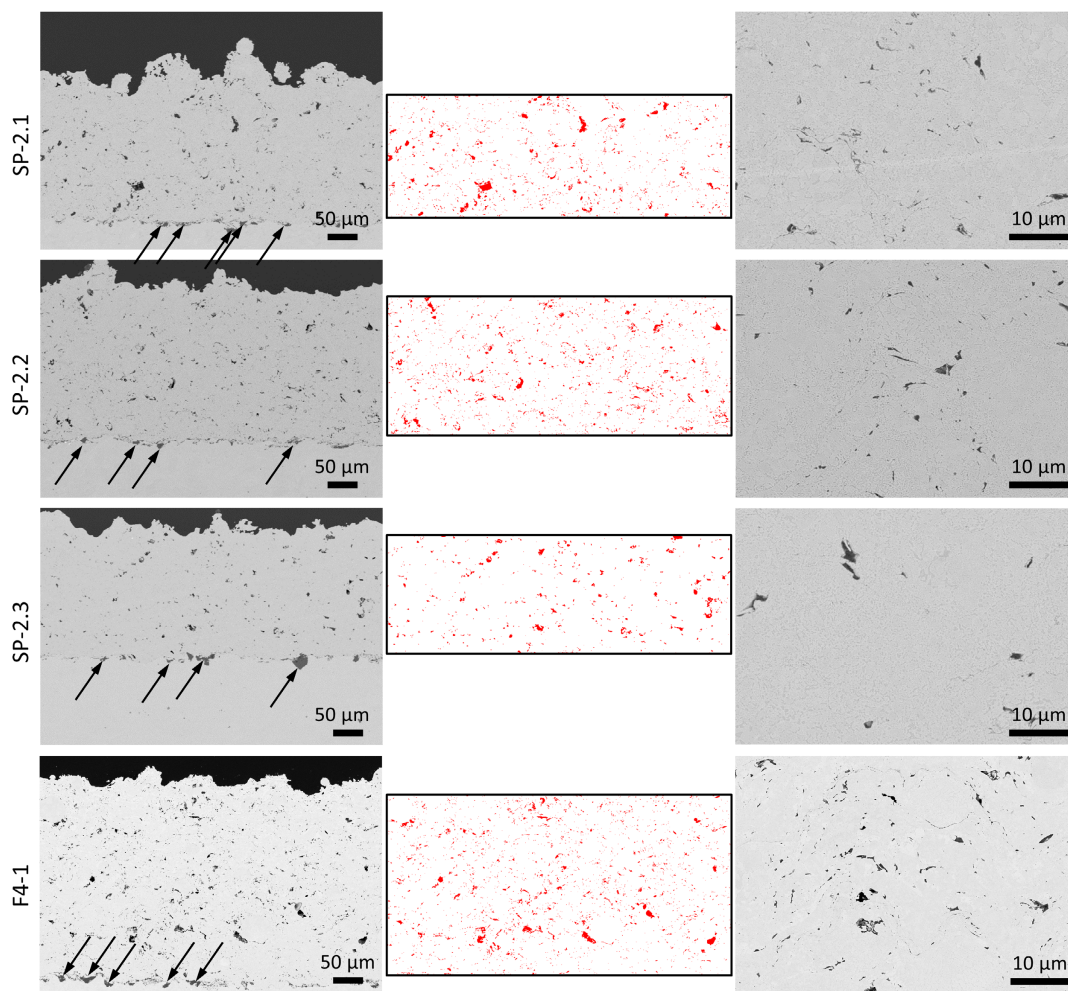


Figure 9. Microstructures of the sprayed samples with the powder Amdry 9954 and parameters SP-2.1, SP-2.2, SP-2.3, and F4-1 (backscattered electron images); arrows indicate alumina particles left behind from blasting; threshold graphs for porosity determination of the images in the left column are given in the middle.

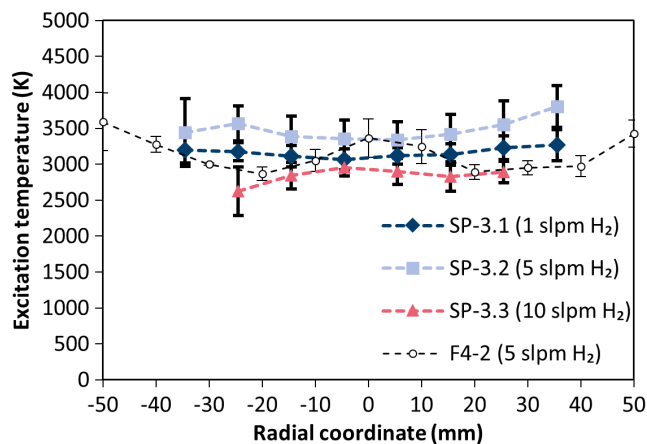


Figure 10. Radial profiles of the excitation temperature at 340 mm downstream from the nozzle for the plasma parameters SP-3.1, SP-3.2, and SP-3.3, and for the reference case F4-2; the error bars represent the uncertainties of the areas under the fit function that were used to represent the emission line intensities.

radial direction as already observed in a previous work.^[25] On the one hand, a mass focusing effect (segregation effect) is reported for supersonic expansions so that the heavier species could be concentrated in the center of the jet.^[30] On the other hand, it was observed that for hydrogen, there is no discontinuity (or jump) in the axial density profile through stationary shock fronts in supersonic jets, which is in contrast to argon. Due to the resulting nonconservation of atomic hydrogen forward flux, H radicals are supposed to escape radially the core of the jet.^[31]

As the hydrogen content increases, the conditions in the plasma deviate from LTE while the electron temperatures are increased via recombination. In contrast, the heavy species temperatures are reduced via an increase in the radial thermal conductivity.^[29] The error bars in Figure 12 representing the uncertainties of the emission line intensities and of the temperatures are indications for such bias to nonequilibrium. This tendency was more pronounced if more hydrogen was added (SP-3.2 and SP-3.3), and always at the jet rims where the electron density was low and thus critical to maintain LTE.

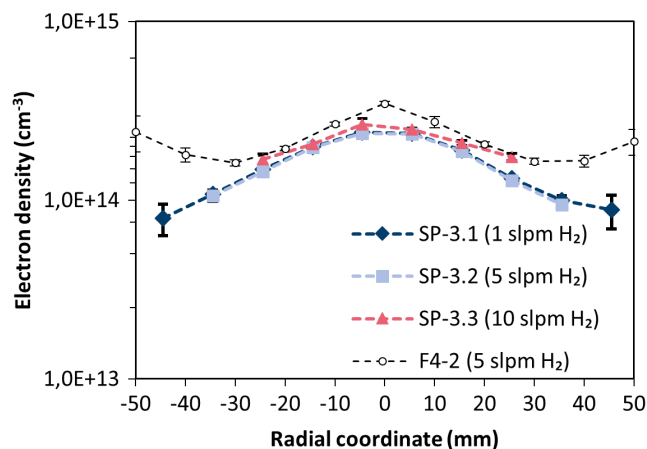


Figure 11. Radial profiles of the electron densities at 340 mm downstream from the nozzle for the plasma parameters SP-3.1, SP-3.2, and SP-3.3, and for the reference case F4-2; the error bars represent the uncertainties of the emission line intensities and the temperatures.

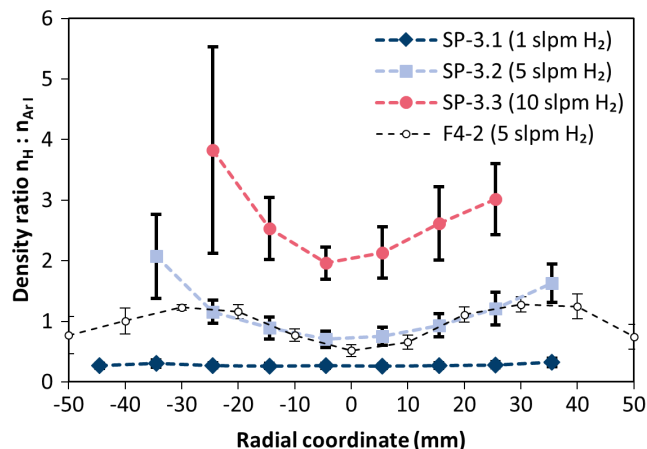


Figure 12. Radial profiles of the hydrogen-argon concentration ratios 340 mm downstream from the nozzle for the plasma parameters SP-3.1, SP-3.2, and SP-3.3, and for the reference case F4-2; the error bars represent the uncertainties of the emission line intensities and the temperatures.

3. Conclusion

In this work, plasma parameters were developed to spray MCrAlY bond coats for high-temperature applications with the novel cascaded single-cathode SinplexPro 03C plasma torch at low pressure. It should be noted that meanwhile, this gun is offered with a 364 W-type nozzle, which is somewhat shorter and has a slightly smaller plasma gas swirl (11° vs 13°) compared to the 301 W-type nozzle used in this work. Besides high deposition efficiencies, dense coatings and low oxygen contents were the main targets. Reference trials were made with the well-established F4-VB gun.

Two parameters turned out to be substantial, the mass-specific plasma enthalpy and the hydrogen-argon plasma gas ratio. Regarding a high deposition efficiency and a low porosity, best

results were achieved at an enthalpy between 17 and 19 MJ kg^{-1} . The oxygen content increased with the enthalpy, however at a degressive tendency.

Already at small hydrogen fractions in the plasma gas, a fast route is established for the recombination of argon ions. Consequently, ionization energy is released and the reactive part of the thermal conductivity is enhanced. This results in an improved thermal treatment of the feedstock. Moreover, the torch input power principally rises if the gun is operated in constant current mode. The oxygen uptake is lowered due to the reducing effect of hydrogen. The highest investigated hydrogen-argon ratio of 0.1 appears advantageous in this regard. Furthermore, the lowest porosity was observed for this parameter. The deposition efficiency did not vary too much by changing the hydrogen content. These results were all obtained at a mass-specific plasma enthalpy of 17 MJ kg^{-1} . The comparison of the coating results obtained with the SP-03C torch with those of the F4-VB gun showed good capabilities of the latter one. In particular, the deposition efficiencies were relatively high and the oxygen contents low. It is assumed that the higher laminarity and the more focused profile of the jet are the reasons for that.

For the SP-03C torch, the deposition efficiency, porosity, and oxygen content were also reasonable if no hydrogen was admixed at all, as the fluctuations of the plasma were effectively reduced. Thus, the perspective opens up to use only argon as plasma gas because this torch can be operated with high currents to reach sufficiently high power even under such conditions. This might be attractive for users who want to avoid the usage of hydrogen and could not have been achieved with the F4-VB gun due to the limitations of the torch power. Further advantages of the cascaded SP-03C torch like an improved long-term stability can be expected, in particular with the Ar-only parameter.

4. Experimental Section

Spray experiments were carried out on a Multicoat LPPS/PS-PVD system (Oerlikon Metco, Wohlen, Switzerland) as mentioned using a SinplexPro 03C torch (SP-03C) with a 301 W-type nozzle (throat diameter of $\frac{1}{2}$ "), powder injection in 20° upstream direction, plasma gas inlet with 13° swirl). For comparison, a F4-VB torch (Oerlikon Metco) with a nozzle throat diameter of 7 mm was used. The process parameters are summarized in Table 1. More details on the selection of the plasma parameters are mentioned below in context with the results. Generally, the spray distances (S/D) were adjusted to the different jet lengths. The torch travel velocity was 440 mm s^{-1} and the raster step was 4 mm.

The feedstocks were the commercially available gas-atomized MCrAlY powders Amdry 386 and Amdry 9954 (Oerlikon Metco, Westbury, NY) with a spherical morphology (Table 2). Both powders are used as a standard for TBCs manufactured in the Jülich Thermal Spray Center and processed with the same spray parameters. Using the F4-VB torch, the carrier gas flow was 1.7 slpm argon through each of the two powder injectors; for the SP-03C torch, this was 3 slpm argon. The powder mass feed rates were 36.6 g min^{-1} for Amdry 386 and 40.1 g min^{-1} for the Amdry 9954 powder. The characteristic particle diameters were determined by laser diffraction (Horiba LA 950 V2, Retsch Technology, Germany) and the oxygen contents by heating in a helium flow and infrared absorption spectroscopy (TCH 600, LECO Corp., St. Joseph, MI, USA). The deposition efficiencies (DE) were calculated based on the powder mass feed rate, sample area, gun motion, and coating weight considering only the spray time when the gun is over the sample and thus excluding overspraying.

Scanning electron microscope investigations (SEM) of the coating microstructures were carried out by means of an Ultra55 system (Carl

Table 2. MCrAlY feedstock powders.

| | Amdry 9954 | Amdry 386 |
|----------------------------------|---|---|
| Nominal composition [by wt%] | Co 32Ni 21Cr 8Al0.5Y | Ni 22Co 17Cr 12Al 0.5Hf 0.5Y 0.4Si |
| d_{10} [μm] | 18 | 16 |
| d_{50} [μm] | 28 | 24 |
| d_{90} [μm] | 43 | 36 |
| Oxygen content [wt%] | 0.0443 ± 0.0014 ($n = 3$) ^{a)} | 0.0400 ± 0.0015 ($n = 4$) ^{a)} |
| Feed rate [g min ⁻¹] | 40.1 | 36.6 |

^{a)}Number of measurements.

Zeiss NTS GmbH, Oberkochen, Germany). For these examinations, the samples were coated with approximately 2 nm platinum. Porosimetry was then accomplished by digital image analysis using the public ImageJ software.^[32] Four to six images per sample were analyzed to validate the results statistically.

Photographs of the plasma jets without powder injection were taken through a borosilicate glass window in the process chamber using a Nikon D300S camera equipped with a 38 mm lens (corresponds to 57 in 35 mm film); the exposure time was 0.125 ms and the aperture was F 22. The images were converted to pseudocolors for better resolution of the jet structure with expansion and compression cells (shock diamonds) being typical for supersonic jets (GNU image manipulation program GIMP 2.10.30).

The spectrometer applied for OES was the ARYELLE 200 model (Laser Technik Berlin [LTB], Berlin, Germany) scanning a wavelength range of 381–786 nm. Plasma radiation was detected through a second borosilicate glass window in the process chamber. The collected radiation was transferred through an achromatic lens and an optical fiber to the 50 μm entrance slit of the spectrometer, and then detected by a 1024 × 1024 CCD array. The system is equipped with an Echelle grating and the spectral resolution capability is 22 000 (17.3–35.7 pm). Calibration was carried out using a spectral Hg lamp. The plasma properties were characterized by intensity and broadening analyses of specific argon and hydrogen

Table 3. Process parameters for OES experiments.

| Set | Current [A] | Ar [slpm] ^{a)} | H ₂ [slpm] ^{a)} | P_{in} [kW] | P_{net} [kW] | h [M] kg ⁻¹ |
|--------|-------------|-------------------------|-------------------------------------|---------------|----------------|--------------------------|
| F4-2 | 650 | 50 | 5 | 41.3 | 23.6 | 15.8 |
| SP-3.1 | 500 | 100 | 1 | 36.7 | 25.5 | 8.6 |
| SP-3.2 | 500 | 100 | 5 | 41.7 | 28.8 | 9.7 |
| SP-3.3 | 500 | 100 | 10 | 45.8 | 29.6 | 9.9 |

^{a)}Standard liters per minute.

Table 4. Results of spray experiments with the feedstock powder Amdry 386.

| Parameter | Porosity [%] | Deposition efficiency [%] | Oxygen content [wt%] |
|-----------|--------------|---------------------------|----------------------|
| F4-1 | 2.45 ± 0.13 | 72.4 | 0.117 ± 0.000 |
| SP-1.1 | 0.86 ± 0.23 | 62.1 | 0.176 ± 0.012 |
| SP-1.2 | 3.39 ± 0.60 | 52.4 | 0.114 ± 0.004 |
| SP-1.3 | 1.36 ± 0.14 | 53.8 | 0.183 ± 0.004 |

Table 5. Results of spray experiments with the feedstock powder Amdry 9954.

| Parameter | Porosity [%] | Deposition efficiency [%] | Oxygen content [wt%] |
|-----------|--------------|---------------------------|----------------------|
| F4-1 | 2.82 ± 0.18 | 68.1 | 0.105 ± 0.001 |
| SP-2.1 | 3.13 ± 0.49 | 39.3 | 0.133 ± 0.005 |
| SP-2.2 | 2.99 ± 0.29 | 50.0 | 0.128 ± 0.013 |
| SP-2.3 | 1.98 ± 0.69 | 28.2 | 0.104 ± 0.011 |

emission lines. The details of this methodology can be found in a previous publication.^[25]

The measurement position for OES was 340 mm from the nozzle exit on various radial distances from the torch axis. **Table 3** gives the process parameters for these experiments. More details on the selection of the plasma parameters are mentioned below in context with the results. **Table 4** and **5** give the numerical results of the spray experiments.

Acknowledgements

The publication of this study was funded by the Deutsche Forschungsgemeinschaft (DFG, German Research Foundation)—491111487. The author gratefully acknowledges Dr. Alexander Barth (Oerlikon Metco) for fruitful discussions, Hiltrud Moitroux for taking the photos, Dr. Doris Sebold for carrying out the SEM work, Mark Kappertz and Michael Xhonneux for preparing the metallographic cross sections, as well as Ralf Laufs for operating the LPPS system (all Forschungszentrum Jülich GmbH, IEK-1).

Open Access funding enabled and organized by Projekt DEAL.

Conflict of Interest

The author declares no conflict of interest.

Data Availability Statement

The data that support the findings of this study are available from the corresponding author upon reasonable request.

Keywords

cascaded plasma torches, low-pressure plasma spraying, MCrAlY bond coats, optical emission spectroscopy

Received: June 14, 2022

Revised: August 24, 2022

Published online: September 18, 2022

- [1] a) J. Toscano, R. Vaßen, A. Gil, M. Subanovic, D. Naumenko, L. Singheiser, W. J. Quadakkers, *Surf. Coat. Technol.* **2006**, 201, 3906; b) D. Naumenko, V. Shemet, L. Singheiser, W. J. Quadakkers, *J. Mater. Sci.* **2009**, 44, 1687.
- [2] P. Song, M. Subanovic, J. Toscano, D. Naumenko, W. J. Quadakkers, *Mater. Corros.* **2011**, 62, 699.
- [3] M. Subanovic, P. Song, E. Wessel, R. Vaßen, D. Naumenko, L. Singheiser, W. J. Quadakkers, *Surf. Coat. Technol.* **2009**, 204, 820.

- [4] A. Gil, V. Shemet, R. Vaßen, M. Subanovic, J. Toscano, D. Naumenko, L. Singheiser, W. J. Quadakkers, *Surf. Coat. Technol.* **2006**, 201, 3824.
- [5] M. Subanovic, D. Sebold, R. Vaßen, E. Wessel, D. Naumenko, L. Singheiser, W. J. Quadakkers, *Mater. Corros.* **2008**, 59, 463.
- [6] a) W. R. Chen, X. Wu, B. R. Marple, D. R. Nagy, P. C. Patnaik, *Surf. Coat. Technol.* **2008**, 202, 2677; b) M. Di Ferdinando, A. Fossati, A. Lavacchi, U. Bardi, F. Borgioli, C. Borri, C. Giolli, A. Scrivani, *Surf. Coat. Technol.* **2010**, 204, 2499; c) G. Mauer, D. Sebold, R. Vaßen, E. Hejrani, D. Naumenko, W. J. Quadakkers, *Surf. Coat. Technol.* **2017**, 318, 114.
- [7] P. Song, D. Naumenko, R. Vaßen, L. Singheiser, W. J. Quadakkers, *Surf. Coat. Technol.* **2013**, 221, 207.
- [8] M. Shibata, S. Kuroda, H. Murakami, M. Ode, M. Watanabe, Y. Sakamoto, *Mater. Trans.* **2006**, 47, 1638.
- [9] B. K. Pant, V. Arya, B. S. Mann, *J. Therm. Spray Technol.* **2007**, 16, 275.
- [10] L. Zhao, M. Parco, E. Lugscheider, *Surf. Coat. Technol.* **2004**, 179, 272.
- [11] B. Rajasekaran, G. Mauer, R. Vaßen, *J. Therm. Spray Technol.* **2011**, 20, 1209.
- [12] G. Mauer, D. Sebold, R. Vaßen, *J. Therm. Spray Technol.* **2014**, 23, 140.
- [13] V. Champagne, D. Helfrich, *Int. Mater. Rev.* **2016**, 61, 437.
- [14] D. L. Guo, D. MacDonald, L. Zhao, B. Jodoin, *J. Therm. Spray Technol.* **2020**, 29, 1628.
- [15] S. B. S. Kalsi, T. S. Sidhu, J. Karthikeyan, H. Singh, *Surf. Eng.* **2015**, 31, 840.
- [16] C. V. Cojocar, M. Aghasibeig, E. Irissou, *J. Therm. Spray Technol.* **2022**, 31, 176.
- [17] G. Mauer, R. Vaßen, D. Stöver, *Surf. Coat. Technol.* **2007**, 201, 4796.
- [18] G. Mauer, K.-H. Rauwald, R. Mücke, R. Vaßen, *J. Therm. Spray Technol.* **2017**, 26, 799.
- [19] Z. Duan, J. Heberlein, *J. Therm. Spray Technol.* **2002**, 11, 44.
- [20] a) J. F. Bisson, C. Moreau, *J. Therm. Spray Technol.* **2003**, 12, 258; b) J. F. Bisson, B. Gauthier, C. Moreau, *J. Therm. Spray Technol.* **2003**, 12, 38.
- [21] a) J. Schein, J. Zierhut, M. Dzulko, G. Forster, K. D. Landes, *Contrib. Plasma Phys.* **2007**, 47, 498; b) J. L. Marqués, G. Forster, J. Schein, *Open Plasma Phys. J.* **2009**, 2, 89.
- [22] K. D. Landes, M. Dzulko, E. Theophile, J. Zierhut, *High Temp. Mater. Processes* **2002**, 6, 10.
- [23] R. Zhukovskii, C. Chazelas, A. Vardelle, V. Rat, *J. Therm. Spray Technol.* **2020**, 29, 3.
- [24] J. Colmenares-Angulo, J. Gutleber, M. Gindrat, A. Pegler, *presented at Inter. Thermal Spray Conf. 2019: New Waves of Thermal Spray Technology for Sustainable Growth*, Yokohama, Japan May, **2019**.
- [25] G. Mauer, *Plasma Chem. Plasma Process.* **2021**, 41, 109.
- [26] M. J. de Graaf, R. P. Dahiya, J. L. Jauberteau, F. J. de Hoog, M. J. F. van de Sande, D. C. Schram, *Colloq. Phys.* **1990**, 51, C5 387.
- [27] R. F. G. Meulenbroeks, R. A. H. Engeln, M. N. A. Beurskens, R. M. J. Paffen, M. C. M. van de Sanden, J. A. M. van der Mullen, D. C. Schram, *Plasma Sources Sci. Technol.* **1995**, 4, 74.
- [28] M. J. de Graaf, R. Severens, R. P. Dahiya, M. C. M. van de Sanden, D. C. Schram, *Phys. Rev. E* **1993**, 48, 2098.
- [29] K. T. A. L. Burm, M. I. Boulous, P. Proulx, B. Jodoin, in *Progress in Plasma Processing of Materials 2001, Proceedings of the 6th European Conference on Thermal Plasma Processes*, Strasbourg, France, May–June, 2000 (Ed: P. Fauchais), Begell House, New York, NY; Wallingford, UK **2001**, pp. 347.
- [30] a) G. Scoles, in *Atomic and Molecular Beam Methods*, Oxford University Pr., New York, NY **1988**; b) R. T. Jongma, T. Rasing, G. Meijer, *J. Chem. Phys.* **1995**, 102, 1925.
- [31] S. Mazouffre, M. G. H. Boogaarts, J. A. M. van der Mullen, D. C. Schram, *Phys. Rev. Lett.* **2000**, 84, 2622.
- [32] W. Rasband, *ImageJ*, National Institutes of Health, Bethesda MD **2022**.